Lab on a Chip

Accepted Manuscript

ROYAL SOCIETY OF CHEMISTRY

www.rsc.org/loc

Magnetically Controllable 3D Microtissues based on Magnetic microcryogels

Wei Liu [a, 1], Yaqian Li [a, 1], Siyu Feng [b], Jia Ning [c], Jingyu Wang[a], Huijun Chen [c], Feng Xu [d], Yanan Du [a, *]

[a] Department of Biomedical Engineering, School of Medicine, Tsinghua University, Beijing, China.

[b] School of Biological Science and Medical Engineering, Beihang University, Beijing, China

[c] Center for Biomedical Imaging Research & Department of Biomedical Engineering, School of Medicine, Tsinghua University, Beijing, China

[d] MOE Key Laboratory of Biomedical Information Engineering, School of Life Science and Technology, Xi'an Jiaotong University, Xi'an, 710049, PR China

[*] Corresponding author: E-mail: duyanan@tsinghua.edu.cn; Fax: +86-10-62773380; Tel: +86-10-62781691

[1] These authors contributed equally to this work.

Abstract

Microtissues on the scale of several hundred microns are promising cell culture configuration resembling the functional tissue units *in vivo*. In contrast to conventional cell culture, handling of microtissues pose new challenges such as medium exchange, purification and maintenance of the microtissue integrity. Here, we developed magnetic microcryogels to assist microtissue formation with enhanced controllability and robustness. The magnetic microcryogels were fabricated on-chip by cryogelation and micro-molding which could endure extensive external forces such as the fluidic shear during pipetting and syringe injection. The magnetically controllable microtissues were applied to constitute novel separable 3D co-culture system realizing functional enhancement of the hepatic microtissues co-cultured with the stromal microtissues and easy purification of the hepatic microtissues for downstream drug testing. The magnetically controllable microtissues with pre-defined shapes were also applied as building blocks to accelerate the tissue assembly process under magnetic force for bottom-up tissue engineering. Finally, the magnetic microcryogels could be injected *in vivo* as cell delivery vehicles and tracked by MRI. The injectable magnetic microtissues maintained viable at the injection site indicating good retention and potential applications for cell therapy. The magnetic microcryogels are expected to significantly promote the microtissues as a promising cellular configuration for cell-based applications such as in drug testing, tissue engineering and regenerative therapy.

Keywords: magnetic nanoparitcles; microcryogels; microtissue; separable co-culture; drug screening

1. Introduction

Living tissues are ensembles of microscale subunits (e.g. lobules in the liver; alveoli in the lung and islets in the pancreas) containing different cell types, extracellular matrices, bioactive soluble factors with well-defined 3D architectures and tissue-specific functions[1]. Regarded with bio-mimicry to the native tissue subunits, *in vitro* engineered microscale tissues (i.e. microtissues) are currently under the spotlight in tissue engineering and regenerative medicine. Due to the microscale precision in architectures and cellular interactions, microtissues outperformed the conventional cell culture configurations (e.g. monolayer culture on planar substrate, dissociated cells, or cell/material mixture) for applications in cell-based drug screening[2-4], organ printing[5, 6], tissue implantation[7, 8] and cell therapy[9, 10].

Microtissues have been engineered via various approaches such as gravity-based hanging-drop method and material-assisted cellular assembly[11]. Material-assisted microtissue formation enables greater flexibilities in tissue architectures compared with the hanging-drop counterpart which usually results in only spherical microtissues. In particular, microscale hydrogel-assisted microtissue formation is widely used to construct tissue-like functional building blocks[1, 12-14], thanks to the good biocompatibility and ease of microfabrication (e.g. micro-molding or photolithography) of the hydrogel[15-17]. Nevertheless, microscale hydrogels suffer from their unsatisfactory load-bearing property, unavoidable cell damage due to crosslinking agents during *in situ* polymerization and lack of controllability of individual microtissue units. Building mechanically robust microtissue units with desirable cellular microenvironment and versatile controllability remains an unmet need in the field of biofabrication and tissue engineering.

In this study, we attempt to build robust and controllable microtissues based on novel magnetic microcryogels, which integrate our recently developed microcryogels[10] with magnetic nanoparticles (MNPs). Microcryogels are microscale macroporous cryogels synthesized on-chip by cryogelation and micro-molding technologies which

could be harvested from the chip and enable automatic and homogenous loading of tailored cellular niches (e.g. cells, matrices, bioactive factors). Compared to microscale hydrogels, microcryogels exhibited excellent elasticity and robustness which could remain intact after being squeezed through the micro-syringe needle[10]. Meanwhile, magnetic nanoparticles (MNPs) have been widely used to enable facile and delicate manipulation of the cells[18] or biomaterials[19] (e.g. microscale hydrogels). And the use of MNPs has been proved as non-toxic and safe for cell labelling (e.g. for cell levitation culture[20]) and as MRI contrast agents approved by U.S. Food and Drug Administration (FDA)[21, 22].

To take advantage of the robustness and magnetic-controllability of the microtissues, we established a separable co-culture system which realized easy co-culture and separation of the functional cells (i.e. HepaRG) and supporting cells (i.e. NIH/3T3 cells) loaded in either magnetic microcryogels or non-magnetic microcryogels. By co-cultured with the NIH/3T3-loaded microtissues, enhanced hepatic functions were achieved for the HepaRG-loaded microtissues, which could be then separated apart for downstream hepatotoxicity drug testing. The magnetic-controllability was further utilized to accelerate the directed assembly of individual microtissue units into larger scale tissue constructs under the external magnetic field. Finally, the MNPs-incorporated microtissues were injected *in vivo* in a site-directed manner to allow their retention tracked by MRI. The robust, controllable and MRI tractable magnetic microtissues are expected to provide solutions to multiple critical issues in tissue engineering and regenerative medicine.

2. Materials and methods

2.1. Materials

Polymethylmethacrylate (PMMA) sheets (0.5mm and 1.0mm thick) were purchased from Sunjin Electronics Co., Ltd. Doxorubicin was purchased from J&K (China). Live/dead assay was purchased from Dojindo Molecular Technologies (Kumamoto, Japan). Cell Titer-Blue was purchased from Promega (Wisconsin, USA). D-luciferin

was purchased from SYNCHEM (Germany). All other reagents were purchased from Sigma-Aldrich (St. Louis, MO) unless otherwise indicated.

2.2. Design and Fabrication of the microstencil array chip

The magnetic microcryogels were generated on the poly-methymetacrylate (PMMA) microstencil array chips (75 cm x 25 cm with thickness of 300 μm), which were designed by CAD software and fabricated by laser prototyping technique using the Rayjet laser system (Rayjet, Australia)[23]. The microstencil chip contained arrays of specific geometries such as circle (with diameters: 400 μm for most of the experiments, 2 mm for mechanical testing and controlled microtissue formation) and clover (for controlled microtissue formation). The microstencil array chips were treated with a Plasma Cleaner (Mycro Technologies, USA) for 2 min in order to increase the hydrophilicity.

2.3. Fabrication of biodegradable magnetic microcryogels and non-biodegradable microcryogels

Two types of microcryogels were fabricated including biodegradable (i.e. gelatin) and non-biodegradable (i.e. PEGDA). M-GMs (Magnetic gelatin microcryogels) were encapsulated with Fe_3O_4 magnetic nanoparticles (MNPs). Briefly, gelatin precursor solution was prepared by dissolving 8 % w/v gelatin powder (extracted from cold water fish, Sigma-Aldrich) and varying MNPs concentration (0, 1, 3, 5% w/v) in deionized water and maintained at 50℃ in water bath. After dissolving adequately, the pre-mixed solution should be incubated on ice for 5 min and then added 0.5% glutaraldehyde (Sigma) and stirred for 20 s. 200 μl precursor solution was pipetted onto the upper surface of the microstencil array chip (600 circle micro-wells with diameter 400 μm) and was evenly distributed by manually scraping with a cover-slide back and forth for several times. The microstencil array chip filled with magnetic gelatin precursor solution was placed in the -20℃ refrigerator and underwent cryogelation for 16 h. The array chips were then lyophilized for 30 min (Boyikang, China). The M-GMs were harvested by a poly-dimethylsiloxane (PDMS) Ejector Pin array and collected by 70 μm cell strainer (BD Biosciences, USA) and then washed with 0.1 M $NaBH_4$ to neutralize uncrosslinked aldehyde, followed by extensive washing with

deionized water. The interconnected macroporous M-GMs were harvested, concentrated into a dish or plate in the shape of monolayer, lyophilized and stored in vacuum for characterization analysis and cell culture. The fabrication of PEGDA-microcryogels without magnetic nanoparticles could follow the previous methods[10].

2.4. Scanning electron microscopy (SEM) and analysis of pore diameter distribution and swelling ratio

The harvested and freeze-dried magnetic microcryogels were gold-coated for 90 s prior to SEM (FEI Quanta 200, USA) imaging for the microstructure evaluation. Meanwhile, the pore diameter distribution of magnetic microcryogel was evaluated and analyzed from SEM imagings of seven different areas using ImageJ software (National Institutes of Health). The equilibrium swelling ratio of the magnetic microcryogels was determined as a ratio of weight of the swollen magnetic microcryogels to the dried magnetic microcryogels. To evaluate the porosity of magnetic microcryogels, the dried M-GMs was hydrated sufficiently and weighed as w1. And then blotting up the held water and weighed as w2. The porosity was calculated as: porosity = (w1-w2)/w1.

2.5. Mechanical testing

To evaluate the effect of MNPs on mechanical properties of the microcryogels, the compression tests were performed using a Bose 3230 mechanical testing machine (Bose, USA). Briefly, M-GMs (Size: diameter = 2 mm; height = 300 μm) were fabricated with different concentration of MNPs (0%, 1%, 3%, 5%) following the above mentioned methods. The unconfined compression tests were performed on a thin sheet constituted by stacking five individual pieces of M-GMs[10]. To compare and analyze the different mechanical properties of M-GMs and hydrogel, magnetic gelatin (8 % w/v) hydrogels (Size: diameter = 8 mm; height = 3 mm) were fabricated by chemical crosslinking (0.5% glutaraldehyde) as previously reported[24]. The stress-strain curve was plotted and the Young's modulus was derived from the linear region of the stress-strain curve. Three parallel samples were performed in each group, and the average values were plotted.

2.6. Degradation test

To demonstrate the biodegradability of the gelatin microcryogel and investigate the effect of the MNPs, the harvested and freeze-dried M-GMs with different concentrations of MNPs (0%, 1%, 3%, 5%) were immersed in the commercially available trypsin/EDTA solution (Gibco, 0.025%). At the predefined time points (t=10, 20, 40, 60, 80, 100, 120, 140 min), the M-GMs were harvested from the solution. The loss of dried weight were measured and calculated based on the formula of the degradation testing[25]. Each measurement was carried out in triplicates.

2.7. Controllability test under fluidic shear stress (FSS)

The poly-methymetacrylate (PMMA) rectangular channel mold (length×width×height=60 mm×2 mm×1 mm) were designed by CAD software and fabricated by laser prototyping technique using the Rayjet laser system. PDMS was casted into the designed mold and cross-linked under 60℃ for 4 h. A hole was drilled at each end of the PDMS channel for inserting capillary tube, allowing fluidic inflow and outflow. The bottom surface of the PDMS channel and a sizeable glass slide were treated by Plasma Cleaner (Mycro Technologies, USA) for 1 min and tightly stuck with each other. A small neodymium magnet (magnet type N38, diameter=8 mm, height=2.5 mm) was placed adjacent to the PDMS channel, providing a magnetic field. Then, M-GMs were injected into the PDMS channel using a 23G syringe. Different scales of fluidic shear stress were applied by adjusting flow rate of a syringe pump (World Precision Instruments, USA). With known channel parameters, flow rates and fluidic viscosity, average shear stress inside the channel could be calculated[26]. The percentage of M-GMs (with MNPs of 1%, 3% and 5%, respectively) immobilized inside the PDMS channel by magnet was recorded when increasing the flow rate. M-GMs with each concentration of MNPs was repeated for five times for statistical analysis.

2.8. Cell culture

Red fluorescent protein (RFP) transfected NIH/3T3 fibroblast cells (RFP3T3) were a gift from Prof. Qin Shen and cultured in Dulbecco's modified Eagle's medium (DMEM) supplemented with 10% fetal bovine serum (FBS) (Wisent Biocenter, Canada). HepaRG cells were cultured in William's E medium (Life technologies, USA)

supplemented with 10% FBS, GlutaMAX™ (Life technologies, USA), 5 μg/ml insulin, 5×10^{-7} M hydrocortisone hemisuccinate, 100,000 U/L penicillin and 100 mg/L streptomycin. HepaRG cells were differentiated in standard medium with 0.5% DMSO for at least 14 days and further cultivation was performed in the presence of 0.5% DMSO. Human adipose-derived mesenchymal stromal cells (hMSCs) were isolated and cultured in the mesenchymal stem cells growth medium (BioWit Technologies, MA, USA) according to previously reported protocol[10]. All cell cultures were maintained at 37 ℃ in a humidified incubator with 5% CO2.

2.9. Cell autoloading into the M-GMs and cell viability/proliferation assessment *in vitro*

Before loading the cells, the harvested and dried magnetic microcryogels in the dish was sterilized by ethylene oxide sterilization system that performed a 12-hour degassing step under vacuum after 12 hours of gas exposure (AN74j/Anprolene, Anderson Sterilization, Inc.Haw River, NC)[27, 28]. Cells were trypsinized and re-suspended in culture medium. 70 μl cell suspension (2×10^6 cells/ml) was subsequently pipetted onto the monolayer constituted tightly by 600 M-GMs in the dish and automatically absorbed into magnetic microcryogels to hydrate the porous structures. And then the dish with the magnetic microcryogels was maintained in a humidified chamber and incubated at 37℃ for 1h to allow for cell attachment.

To assess cell viability and cell proliferation, magnetic microcryogels with different concentrations of magnetic nanoparticles (1%, 3%, 5%) were seeded with NIH3T3 and cell viability was assessed by CellTiter-Blue at day1, day4, day7. Live/dead assay was also performed for visualization of cell viability by Nikon fluorescence microscopy.

2.10. Separable co-culture system

Green fluorescent protein (GFP) transfected HepaRG (GFP^+-HepaRG) cells were cultured in the flask and differentiated using 0.5% DMSO for 2 weeks before further experiment. Differentiated GFP^+-HepaRG cells were trypsinized and 60μl cell suspension ($5x10^6$/ml) was loaded into 600 PEGDA microcrogels. The PEGDA

microcryogels loaded with GFP^+-HepaRG were cultured for 5 days in the presence of 0.5% DMSO before co-culture. 600 M-GMs (with 3% MNPs) were loaded with 70μl NIH3T3 cell suspension and cultured for one day. The prepared M-GMs with NIH3T3 and PEGDA microcryogels with GFP^+-HepaRG were mixed and co-cultured for 7 days in the 24-well culture plate. At the end of co-culture, a cylindrical neodymium magnet was placed on the reverse side of the plate in order to apply magnetic force vertically to the plate, and the M-GMs with NIH3T3 was fixed. After that, the PEGDA microcryogels with GFP^+-HepaRG could be separated through simply pipetting from the mixture and applied for further drug testing.

2.11. Evaluation of the liver functions

Secreted human albumin and urea synthesis by HepaRG cells in the culture medium were collected at day 3 and day 7. Urea synthesis was quantified by QuantiChrom™ Urea Assay Kit (BioAssay Systems, USA) and human albumin was quantified by enzyme-linked immunosorbent assay (ELISA) using commercially available test kits (Bethyl Laboratory, Montgomery, TX, USA).

2.12. Fabrication of cell-laden magnetic microcryogel-based microtissues

M-GMs were loaded with NIH3T3 cell and cultured in the cell culture plate. The cylindrical neodymium magnets were placed on the surface of the plate and the magnetic microcryogels tightly conglomerated to grow into each other. Special shapes of magnetic microcryogels were fabricated to form controlled microtissues. Circle and clover shaped magnetic microcryogels were loaded with RFP3T3. Magnetic microcryogels were thoroughly mixed and cultured in the cell culture plate with cylindrical neodymium magnets on reverse side of the plate. After culture for 10 days, RFP3T3 cells within the macro-scale tissue assembly were observed by fluorescence microscope.

2.13. MRI analysis and Bioluminescence imaging

To track cells in *vivo*, hMSCs were infected with firefly luciferase and enhanced GFP (Luc^+ EGFP) by lentiviruses according to the previous method[10] and the positive rate could reach more than 90%. The magnetic microcryogels

with 3% MNPs were loaded with Luc^+ hMSCs (~500 cells/microcrygel) and cultured in 5% CO_2 incubator at 37 °C for 1 day.

BALB/c nude mice (20-25 g, 4-6 weeks) were used for the *in vivo* studies. All the animal experiments were performed under a strict protocol approved by the Animal Ethics Committee on the Center of Biomedical Analysis, Tsinghua University. Mice were anesthetized using 2% isoflurane and 200 magnetic microcryogels with Luc^+ hMSCs in 200 μl 15% gelatin solution (to suspend M-GMs homogeneously) were injected in the left gracilis muscle[29]. Meanwhile, the blank gelatin microcryogels without MNPs and Luc^+ hMSCs was injected into the same site of the right limb in the same mouse. Then the samples were detected by MRI at days 1, 5, and 10. Scanning was conducted by a 3T scanner (Achieva TX, Philips Medical System, Best, Netherland) with an animal coil (Chengguang Cooperation, Shanghai, China). Three dimension T2 weighted TSE[30] sequence was employed to track the M-GMs with scan parameters: TE/TR, 251/2900ms; echo train length, 80; flip angle, 90; spatial resolution, 0.23×0.23×1mm; Field of View, 120×49.6×20 mm NSA (number of acquisition: 6).

Bioluminescence imaging was also performed to track the cell retention and cell viability on days 1, 5, 10 after injection using a Xenogen IVIS Lumina Ⅱ imaging system (Caliper Life Sciences, USA).

2.14. Statistical analysis

Quantitative data were presented as means ± standard deviations (s.d.). Statistical analysis was performed using one-way ANOVA. A value of $P < 0.05$ was considered to be statistically significant.

3. Results

3.1. Fabrication and characterization of the magnetic microcryogel

We fabricated the magnetic microcryogels in a microstencil array chip based on our previously developed microcryogel technology[10], by physical encapsulation of the MNPs during cryogelation. Individual microcryogels in the microstencil array chip were harvested by sandwiching with a PDMS Ejector Pin array made by standard

soft lithography. Magnetic microcryogels could be easily collected and concentrated by filtering through a cell strainer (Fig. 1A). Microcryogels were well-known for their interconnected macroporous structures with pore sizes in the range of 20-80 μm[10]. To evaluate the effect of encapsulated MNPs on the microstructure of magnetic gelatin microcryogels (M-GMs,) SEM imaging of the magnetic microcryogels with 0%, 1%, 3%, 5% MNPs was performed revealing homogenous encapsulation of the MNPs into the laminate structure of the macroporous microcryogels (Fig. 2A). Pore size distribution analyzed by NIH ImageJ showed that the pore size of microcryogels containing 0% MNPs was mainly in the range of 50-80 μm, while the pore size of microcryogels containing 3% and 5% MNPs were mainly in the range of 10-50 μm (Fig. 2B). This indicated that the encapsulated MNPs might occupy the pore structures of magnetic microcryogels leading to decreasing the pore size.

Meanwhile, the macroporous M-GMs exhibited high porosity (>90%) and swelling ratio (>15). Comparing to the microcryogels containing 0% MNPs, the porosity and swelling ratio of the M-GMs containing 3% and 5% MNPs were decreased (Fig. 3A, B), and there was no statistically significant difference between the microcryogels containing 0% MNPs and 1% MNPs. Since the porosity and swelling ratio depend on both the pore size of the polymer network and the polymer-solvent interactions[31], high concentration of MNPs may reduce the porosity and swelling ratio of the M-GM by decreasing the pore size of the scaffold.

Next, we evaluated whether the gelatin microcryogel with MNPs preserved inherent enzymatic degradability of gelatin. The degradation of M-GM *in vitro* was measured based on the decreased weight in the presence of 0.025% trypsin/EDTA solution. All the groups of the samples could be degraded within about 90 min (Fig. 3C) indicating good biodegradability of the M-GMs.

We then analyzed the effect of MNPs on the mechanical properties of the microcryogels, which is well-known for the excellent load-bearing capacity. There was no statistical difference in the Young's modulus of microcryogels with different concentrations of MNPs (Fig. 3F). Compared with the magnetic gelatin hydrogels, M-GMs

exhibited lower Young's modulus (159.5Pa in M-GMs vs 247.4Pa in magnetic hydrogels) (Fig. 3D, E). The magnetic hydrogel was fractured when subjected to 61% compress strain. In contrast, the M-GMs remained intact even under deformation above 80% (Fig. 3D. Supplementary video S1). The data revealed the excellent elasticity and load-bearing properties of the M-GMs superior to the magnetic hydrogels.

3.2. Magnetic controllability assessment under shear stress

In order to test the magnetic controllability of M-GMs under shear stress, we built PDMS rectangular channels, providing different scales of fluidic shear stress (Fig. 4A-B). M-GMs with MNPs of 1%, 3% and 5% were tested respectively for their retention under magnetic field in fluidic shear indicating by bearable shear stress (Fig. 4C.Supplementary video S2). As expected, both the 50% bearable shear stress (Fig. 4D) (half of M-GMs could be stabilized by external magnet under certain shear stress) and the 100% bearable shear stress (Fig. 4E) were enhanced as the MNPs concentration increased. As shown in Fig. 4D, the 50% bearable shear stress for the 3% MNP microcryogels was 8 dynes /cm^2 which equals to the magnitude of shear stress generated by physiological blood flow. Furthermore, the 50% bearable shear stress of 5% Fe-G-MC was 25.6 dynes /cm^2 (several times higher than the physiological shear stress). Therefore we may module the controllability of the M-GMs for applications in high stressed *in vitro* or *in vivo* environment through increasing the MNPs concentration.

3.3. Cell compatibility of magnetic microcryogels

To evaluate cell compatibility of the magnetic microcryogels, NIH3T3 cells were seeded into M-GMs with different concentration of MNPs (1%, 3%, 5%). As shown in the schematic (Fig. 1C), the cells could be automatically loaded into the macroporous magnetic microcryogels by simply pipetting onto the surface of collected M-GMs from the chips. Even distribution, firm attachment and continuous proliferation were achieved for NIH3T3 cells during 7 days' culture in the M-GMs with different concentrations of MNPs (Fig. 5A-B). A slight degree in cell seeding efficiency was observed with increasing MNP concentration probably due to occupation of

pore structures by the MNPs. However, the proliferation rate was consistent in different concentrations of MNPs all reaching more than 1000 cells per gel after 7 days' culture. The results indicated that the incorporation of MNPs into magnetic microcryogels did not pose any negative effect on the biocompatibility of the microcryogels, which could be used as desirable cellular micro-niches.

In general, M-GMs with 3% MNPs exhibited desirable material properties (i.e. pore size, porosity and swelling ratios), excellent magnetic controllability under shear stress and satisfactory cellular biocompatibility, which was chosen for the following applications.

3.4. Separable co-culture system and enhanced HepaRG function after co-culture with NIH3T3

To demonstrate the application of the magnetic microcryogels, a novel separate 3D co-culture system was established with cells loaded in both magnetic and non-magnetic microcryogels respectively. Hepatic cells (HepaRG) and stromal fibroblast cells (NIH3T3 cells) were co-cultured to enhance the liver functions of Hepatic cells by supporting fibroblasts. The co-cultured HepaRG microtissues could be easily separated with the supporting microtissues using a magnet (Fig. 6A-B) which could be applied for downstream drug testing. We applied non-adhesive PEGDA microcryogels developed previously[10] to support HepaRG cell growth which exhibited spheroidal morphology and applied the M-GMs to generate stromal microtissues. During co-culture, cells within the microtissues did not migrate into another type of microtissues. After 7 days' co-culture, HepaRG spheroids were formed in both co-culture and mono-culture microcryogels with larger spheroids formed in the co-culture (Fig. 6C). Liver functions including albumin expression and urea synthesis were significantly higher in co-culture compared to HepaRG mono-culture (Fig. 6D-E). It is well-known that liver functions of hepatocytes gradually weaken *in vitro* under conventional 2D culture conditions[32]. Our results showed that liver function of HepaRG cells could be preserved in 3D microtissues due to tight cell-cell contact and be further elevated by co-culture with supporting stromal microtissues.

The HepaRG microtissues could be easily separated with the magnetic stromal microtissue by using a magnet and the purified hepatic microtissues were subjected to drug testing of Doxorubicin (DOX), a well-known anti-cancer drug metabolized in the liver by efflux drug transporter *P*-glycoprotein (MDR1)[33]. After Dox treatment for 24 h, the 50% inhibition concentration (IC50) of Dox against HepaRG cells after co-culture (17.229μM) was higher than that of the HepaRG mono-culture (6.033μM) (Fig. 6F). The elevated IC50 may be explained by enhanced drug metabolic functions of HepaRG microtissues after co-culture which led to higher drug resistance. Moreover, the microtissues all maintained intact during the entire handling process (e.g. medium exchange, staining, washing, magnetic separation and drug testing) benefited from the robustness of the magnetic microcryogels.

3.5. Accelerated and controllable microtissue assembly for bottom-up tissue engineering

Another unique advantage of magnetic controllability is to accelerate the microtissue assembly for bottom-up tissue engineering. Two formats, namely random or directed assembly, were designed to illustrate the efficiency and controllability of the microtissue assembly (Fig. 7A). Magnetic microtissues loaded with RFP-3T3 could be quickly agglomerated by placing a magnet on top of the micro-well culture plate which formed connection through cell growth and migration between neighboring microtissues as early as day 5. After 7 days' culture, the individual microtissue building blocks were merged with each other and the whole assemble became inseparable at day 10 (Fig. 7B, C). In comparison, in the absence of the magnet, scattered magnetic microtissue building blocks were observed with minimum connections at day 10, even when the microtissue building blocks were seeded at high density to guarantee close proximity. To further illustrate the controllability of magnetic microtissues, we designed circle- and clover- shaped magnetic microcryogels inspired by the 'lock-and-key' design[1] to direct the microtissue assembly (Fig. 7A). As shown in Fig. 7D, the two types of the magnetic microcryogels could self-organize and assemble into a monolayer under horizontal shaking and vertical magnetic field, with each clover shaped M-GM surrounded by four circle-shaped M-GMs. The assembled M-GMs loaded with RFP-3T3 merged with each other

to form connected macrotissue sheet after 10 days.

3.6. Injectable magnetic microtissue tracked by MRI and Bioluminescence *in vivo.*

The magnetic microcryogels could be readily injected as cell delivery vehicles *in vivo* for cell-based therapy which could be detected by magnetic resonance imaging (MRI) to achieve microtissue tracing. As a prove-of-concept of microtissue tracing, 300 M-GMs auto-loaded with luciferase-transduced hMSC (Luc^+ hMSC) were intramuscularly injected into the gracilis muscle in the left limb of BALB/c nude mice. As control, gelatin microcryogels without MNPs loaded with Luc^+ hMSC were injected into the corresponding site in the right limb. Owing to the MNPs, hypointense MRI signals could be detected for the M-GMs which remained for at least 10 days (Fig. 8A). To confirm the presence and long-term survival of cells in the magnetic microcryogels, bioluminescence generated by the Luc^+ hMSCs were constantly visualized for 10 days by a live animal imaging system indicating stable retention and sustained viability of the cells at the injection site (Fig. 8B). As expected, the blank gelatin microcryogels generated no signals detected by either MRI or live animal imaging system. Our data presented potential tracking approach for *in vivo* cell therapy based on microtissues by MRI-imaging the MNPs entrapped in delivery vehicle.

4. Discussion

Currently, *in vitro* engineered microtissues were promising cell culture configuration to mimic the functional tissue units *in vivo*, which can be fabricated via various approaches such as gravity-based hanging-drop method and material-assisted cellular assembly. The unmet need in microtissue engineering is to fabricate mechanically robust microtissue units with desirable cellular microenvironment and versatile controllability. Thanks to the excellent load-bearing property of microcryogels, the microtissues could endure extensive forces applied externally such as the fluidic shear force during pipetting and syringe injection. In a fluidic-based test, the magnetic microcryogels could be stably anchored using a common magnet under the fluidic stress as high as 14.58 dynes/cm^2 (Fig. 4), which is about twice higher than the shear force generated by physiological blood flow. The robustness and

controllability of the magnetic microcryogles lead to convenient manipulation of the microtissues eliminating potential cell loss during medium exchange, guarantee microtissue integrity during long-term culture and allow magnetic purification of desired functional units.

In native tissues, homotypic and heterotypic cell-cell interactions play fundamental role in maintaining tissue physiology and functions[32]. Co-culture of multiple cell types are widely used to enhance the cellular functions by recreating the synergistic cellular interactions. Most co-culture systems are based on cells maintained on 2D substrate such as the widely-used Transwell system and micropatterned systems[34, 35]. 3D co-culture systems (e.g. in the format of multicellular spheroids[36], cell-laden microgels[1, 37] or multi-layered cell sheets[32]) are emerging to provide more biomimetic and enhanced homotypic and heterotypic cellular interactions. However, 3D co-cultured microtissues are currently inseparable thus limit their downstream applications (e.g. drug screening or cell therapy) which usually demand purified cell population. Our magnetic-controllable microcryogels accomplished separable co-culture of microtissues loaded with hepatic cells and stromal fibroblasts. Enhanced liver functions were obtained for the hepatic microtissues which could be easily separated from the stromal microtissues and subjected to following drug treatment. No visible cross-contamination of the two types of cells was observed thanks to the high molecular/cell adhesion resistance of PEG-based microcryogels[10]. The separable co-culture systems based on microtissues can be integrated into the bioreactor in the future to achieve large-scale microtissue production. In this regard, the robustness of the microtissues achieved here is extremely vital to endure the tremendous fluidic shear during mixing in the bioreactors. Meanwhile, the magnetic microcryogel-based 3D co-cultured platform can be readily applied for other cell types as desirable *in vitro* model to investigate cellular interactions on the tissue level and as functional cellular agents for drug screening and regenerative therapy.

Another promising application of the magnetic microtissues is as building blocks for bottom-up tissue engineering, which can be assembled into macroscale tissue constructs with clinically-relevant geometries. Currently, numerous

assembly approaches have been utilized to assemble cell-laden microscale hydrogels for building macroscale tissue-like constructs such as microfluidics[38], acoustic[39], hydrophilic-hydrophobic interactions, or magnetic force[12, 40]. Here we showed the importance of magnetic force to accelerate microcryogel-based microtissue assembly and the resulting macro-tissue construct. Microcryogels with more diverse shapes mimicking natural microarchitectures will be designed to generate more physiologically relevant tissue construct. Besides, MNPs entrapped in microcryogels could be tracked *in vivo* by MRI to locate the residence of the microtissues. MRI and BLI imaging demonstrated that the magnetic signal could be detected at least 10 days after implantation indicating good cell retention and maintenance of viability. MNPs were entrapped in microcryogels instead of within cells, therefore the MRI signals were determined by the degradation rate of microcryogels other than cells. Consequently, magnetic microcryogels may be directly injected in desired physiological sites guided by MRI and retained with great stability by applying a magnetic field. The site-directed delivery and retention of microtissue are particularly significant for body sites with high pressure, high shear stress and cavities (e.g. bladder, stomach or intervertebral disk). In the future, the magnetically-separated functional microtissues enhanced by co-culturing with supporting microtissues can be further assembled into complex tissue construct as *in vitro* model or injected into particular disease sites to perform therapeutic functions *in vivo*.

5. Conclusion

We fabricated magnetic microcryogels on chip to assist 3D microtissue formation with improved robustness and controllability. The magnetic microcryogels lead to convenient manipulation of the microtissues which eliminates potential cell loss during medium exchange, guarantee microtissue integrity during long-term culture and allow magnetic purification of desired functional units. The magnetic microtissues were applied to establish a separable co-culture system to control and enhance hepatic microtissues functions for downstream drug testing. With the assist of external magnetic force, accelerated assembly of shape-controlled magnetic microtissues were achieved

resulting in macro-scale tissue constructs. Finally, we proved potential application of magnetic microcryogels as injectable cell delivery vehicles which could be tracked *in vivo* by MRI for cell-based therapy.

Acknowledgements

We thank Prof. Wei Sun for providing the mechanical testing machine and Liliang Ouyang's help of the mechanical testing and all Du lab members for general assistance. This work is financially supported by the Natural Science Foundation of China (81171474, 51273106, 11372243).

References

1. Y. Du, E. Lo, S. Ali and A. Khademhosseini, *Proc Natl Acad Sci U S A*, 2008, 105, 9522-9527.
2. C.-T. Ho, R.-Z. Lin, R.-J. Chen, C.-K. Chin, S.-E. Gong, H.-Y. Chang, H.-L. Peng, L. Hsu, T.-R. Yew, S.-F. Chang and C.-H. Liu, *Lab on a Chip*, 2013.
3. X. Li, X. Zhang, S. Zhao, J. Wang, G. Liu and Y. Du, *Lab Chip*, 2014, 14, 471-481.
4. S. Zhao, H. Zhao, X. Zhang, Y. Li and Y. Du, *Lab Chip*, 2013, 13, 2350-2358.
5. C. Norotte, F. S. Marga, L. E. Niklason and G. Forgacs, *Biomaterials*, 2009, 30, 5910-5917.
6. D. Wang, D. Cheng, Y. Guan and Y. Zhang, *Biomacromolecules*, 2011, 12, 578-584.
7. J. M. Kelm, V. Djonov, L. M. Ittner, D. Fluri, W. Born, S. P. Hoerstrup and M. Fussenegger, *Tissue Eng*, 2006, 12, 2151-2160.
8. T. H. Petersen, E. A. Calle, L. Zhao, E. J. Lee, L. Gui, M. B. Raredon, K. Gavrilov, T. Yi, Z. W. Zhuang, C. Breuer, E. Herzog and L. E. Niklason, *Science*, 2010, 329, 538-541.
9. G. J. Delcroix, P. C. Schiller, J. P. Benoit and C. N. Montero-Menei, *Biomaterials*, 2010, 31, 2105-2120.
10. W. Liu, Y. L, Y. Zeng, X. Zhang, J. Wang, L. Xie, X. Li and Y. Du, *Acta Biomater*, 2014.DIO: http://dx.doi.org/10.1016/j.actbio.2013.12.008
11. S. Nola, J. C. Erasmus and V. M. Braga, *Methods Mol Biol*, 2012, 827, 143-155.
12. F. Xu, C. A. Wu, V. Rengarajan, T. D. Finley, H. O. Keles, Y. Sung, B. Li, U. A. Gurkan and U. Demirci, *Adv Mater*, 2011, 23, 4254-4260.
13. H. Qi, M. Ghodousi, Y. Du, C. Grun, H. Bae, P. Yin and A. Khademhosseini, *Nat Commun*, 2013, 4, 2275.
14. F. Xu, F. Inci, O. Mullick, U. A. Gurkan, Y. Sung, D. Kavaz, B. Li, E. B. Denkbas and U. Demirci, *ACS Nano*, 2012, 6, 6640-6649.
15. J. H. Sung, J. Yu, D. Luo, M. L. Shuler and J. C. March, *Lab Chip*, 2011, 11, 389-392.
16. G. Y. H. Y.H. Li, X.H. Zhang, B.Q. Li, Y.M. Chen, T.L. Lu, T.J. Lu, F. Xu, *Advanced Functional Materials*, 2013, 23, 660–672.
17. Y. L. Han, Y. Yang, S. Liu, J. Wu, Y. Chen, T. J. Lu and F. Xu, *Biofabrication*, 2013, 5, 035004.
18. H. J. Chung, H. Lee, K. H. Bae, Y. Lee, J. Park, S. W. Cho, J. Y. Hwang, H. Park, R. Langer, D. Anderson and T. G. Park, *ACS Nano*, 2011, 5, 4329-4336.
19. Y. Dai, P. Ma, Z. Cheng, X. Kang, X. Zhang, Z. Hou, C. Li, D. Yang, X. Zhai and J. Lin, *ACS Nano*, 2012, 6, 3327-3338.

20. G. R. Souza, J. R. Molina, R. M. Raphael, M. G. Ozawa, D. J. Stark, C. S. Levin, L. F. Bronk, J. S. Ananta, J. Mandelin, M. M. Georgescu, J. A. Bankson, J. G. Gelovani, T. C. Killian, W. Arap and R. Pasqualini, *Nat Nanotechnol*, 2010, 5, 291-296.
21. W. Chen, P. Yi, Y. Zhang, L. Zhang, Z. Deng and Z. Zhang, *ACS Appl Mater Interfaces*, 2011, 3, 4085-4091.
22. A. P. Khandhar, R. M. Ferguson and K. M. Krishnan, *J Appl Phys*, 2011, 109, 7B310-317B3103.
23. Y. G. Kim, S. Moon, D. R. Kuritzkes and U. Demirci, *Biosens Bioelectron*, 2009, 25, 253-258.
24. M. B. Dainiak, I. U. Allan, I. N. Savina, L. Cornelio, E. S. James, S. L. James, S. V. Mikhalovsky, H. Jungvid and I. Y. Galaev, *Biomaterials*, 2010, 31, 67-76.
25. M. Jurga, M. B. Dainiak, A. Sarnowska, A. Jablonska, A. Tripathi, F. M. Plieva, I. N. Savina, L. Strojek, H. Jungvid, A. Kumar, B. Lukomska, K. Domanska-Janik, N. Forraz and C. P. McGuckin, *Biomaterials*, 2011, 32, 3423-3434.
26. Y. Son, *Polymer*, 2007, 48, 632-637.
27. S. Ohya and T. Matsuda, *J Biomater Sci Polym Ed*, 2005, 16, 809-827.
28. X. Guo, H. Park, S. Young, J. D. Kretlow, J. J. van den Beucken, L. S. Baggett, Y. Tabata, F. K. Kasper, A. G. Mikos and J. A. Jansen, *Acta Biomater*, 2010, 6, 39-47.
29. J. Qin, K. Li, C. Peng, X. Li, J. Lin, K. Ye, X. Yang, Q. Xie, Z. Shen, Y. Jin, M. Jiang, G. Zhang and X. Lu, *Biomaterials*, 2013, 34, 4914-4925.
30. S. H. W. Xiangyang Shi, Scott D. Swanson, Song Ge, Zhengyi Cao, Mary E. Van Antwerp, Kevin J. Landmark,andJames R. Baker, Jr, *Advanced Materials*, 2008, 20, 1671-1678.
31. E. S. Gil, D. J. Frankowski, R. J. Spontak and S. M. Hudson, *Biomacromolecules*, 2005, 6, 3079-3087.
32. A. Ito, H. Jitsunobu, Y. Kawabe and M. Kamihira, *J Biosci Bioeng*, 2007, 104, 371-378.
33. M. Le Vee, E. Jigorel, D. Glaise, P. Gripon, C. Guguen-Guillouzo and O. Fardel, *Eur J Pharm Sci*, 2006, 28, 109-117.
34. S. R. Khetani and S. N. Bhatia, *Nat Biotechnol*, 2008, 26, 120-126.
35. E. E. Hui and S. N. Bhatia, *Proc Natl Acad Sci U S A*, 2007, 104, 5722-5726.
36. H. F. Lu, K. N. Chua, P. C. Zhang, W. S. Lim, S. Ramakrishna, K. W. Leong and H. Q. Mao, *Acta Biomater*, 2005, 1, 399-410.
37. B. Zamanian, M. Masaeli, J. W. Nichol, M. Khabiry, M. J. Hancock, H. Bae and A. Khademhosseini, *Small*, 2010, 6, 937-944.
38. S. E. Chung, W. Park, S. Shin, S. A. Lee and S. Kwon, *Nat Mater*, 2008, 7, 581-587.
39. F. Xu, T. D. Finley, M. Turkaydin, Y. Sung, U. A. Gurkan, A. S. Yavuz, R. O. Guldiken and U. Demirci, *Biomaterials*, 2011, 32, 7847-7855.
40. O. Ziv-Polat, H. Skaat, A. Shahar and S. Margel, *Int J Nanomedicine*, 2012, 7, 1259-1274.

Figure legends

Fig. 1 Schematic demonstration of fabrication, magnetic controllability assessment and three exemplary applications of the magnetically-controllable 3D microtissues. (A) Fabrication of the magnetic microcryogels from the microstencil array chip; (B) Magnetic controllability assessment under shear stress *in vitro*; (C) Cells were auto-loaded into the magnetic microcryogels; (D) Separable co-culture system for function enhancement of the microtissues which can be used for downstream drug testing; (E) Accelerated and controllable microtissue formation by random and shape-directed assembly; (F) *In vivo* tracking of microtissues by MRI.

Fig. 2 Scanning electron microscopy (SEM) images and pore size statistics of the magnetic microcryogels. (A) The SEM images of MNPs (0%, 1%, 3%, 5%) encapsulated microcryogels showing the MNPs were uniformly distributed in the interconnected and macroporous structures. (B) The pore size distribution of the magnetic microcryogels with different concentrations (0%, 1%, 3%, 5%) of the MNPs. Data are means ± SEM; n =3

Fig. 3 Characterization of the magnetic microcryogels: (A-B) The porosity quantification by Image J software and swelling ratio of the MNPs (0%, 1%, 3%, 5%) encapsulated microcryogels. (C) Degradation rate of the magnetic microcryogels with different concentrations of MNPs. (D) Strain-stress curves of 3% MNPs encapsulated hydrogel and magnetic microcryogels respectively subjected to compression tests. (E) Comparison of Young's modulus between the magnetic hydrogel and magnetic microcryogel by the strictly linear region of the stress-strain curve (D). (F) Young's modulus of the MNPs (0%, 1%, 3%, 5%) encapsulated microcryogels. Data are means ± SEM; n = 3**.**

Fig.4 The controllability assessment of magnetic microcryogels under shear stress in vitro: (A-B) Schematics and photographs of the microfluidic device for controllability assessment. (C) The immobilized ratio of the magnetic microcryogels with different concentrations of MNPs under different sheer stress. (D-E) The relation between MNPs concentration and bearable maximum shear stress. The bearable shear stress of 50% M-GMs and bearable shear stress of 100% M-GMs were enhanced as the MNPs concentration increased. Data are means ± SEM; n = 3.

Fig. 5 Cell viability and proliferation within the magnetic microcryogels with different concentrations of MNPs. (A) Live/dead assay of NIH3T3 in the magnetic microcryogels after culturing for 1, 4, and 7 days. Viable cells are green and dead cells are red. (B) Quantitative assessment of cell proliferation rate at different time. Scale bar=200 μm. Data are means ± SEM; n = 3.

Fig. 6 The separable co-culturing system and downstream application for drug testing. (A) Schematic demonstration of the separable co-culturing system. Two types of cells were seeded into non-magnetic microcryogles and magnetic microcryogels respectively. After co-culturing for desired days, the magnetic microcryogels were immobilized and separated from non-magnetic microcryogels simply by using a magnet. The two types of microcryogels could be applied to further downstream applications. White cylinders represent non-magnetic microcryogels and grey black cylinders represent magnetic microcryogels. (B) Photographs of separable co-culturing system. HepaRG cells were chosen to co-culture with stromal fibroblasts (RFP3T3) to enhance hepatic functions. HepaRG cells were seeded into PEGDA microcryogels and RFP3T3 were seeded into

gelatin magnetic microcryogels. After co-culturing for 7 days, HepaRG cells loaded in PEGDA microcryogels were purified by pipetting and applied for Dox testing. (C) Bright-field and fluorescence images of the two types of microcryogels mixed together. (PM, PEGDA microcryogels; M-GM, magnetic gelatin microcryogels) Scale bar=200 μm. (D, E) Urea production and ALB secretion rate of HepaRG cells co-cultured with RFP3T3 for 7 days. Data are means ± SEM; n = 3. (F) Cytotoxicity testing of Dox on co-cultured HepaRG microtissues showing increased IC50 as compared with the mono-cultured HepaRG microtissues. Data are means ± SEM; n = 3.

Fig. 7 Magnetically-driven microtissue assembly for bottom-up tissue engineering. (A) Schematic illustration of construction of macro-scale tissues by random or shape-directed assembly of the magnetic microcryogels. Top panel: cells were loaded into the gelatin magnetic microcryogles and randomly assembled to form tissue aggregation under magnetic force. Bottom panel: magnetic microcryogels with specific geometries were assembled under external magnetic force. (B, C) Photographs and fluorescence images of random microtissues assembly in the presence or absence of the magnet. Cells were labeled using live/dead assay. Scale bar=200 μm. (D) Shape-directed microtissue assembly. Photographs of circle and clover magnetic microcryogels and fluorescence images of the shape-directed microcryogels assembly (Red, RFP3T3 cells).

Fig. 8 Injectable microtissues tracked in vivo by both MRI and BLI. (A) MRI monitoring the magnetic signals of the injected magnetic microcryogels for 10 days in the left leg of mouse. Arrows indicate the injection site of the magnetic microcryogels. (B) Luc+ hMSCs were loaded into the magnetic microcryogels and visualized by bioluminescence imaging (BLI) showing good cell viability for up to 10 days.

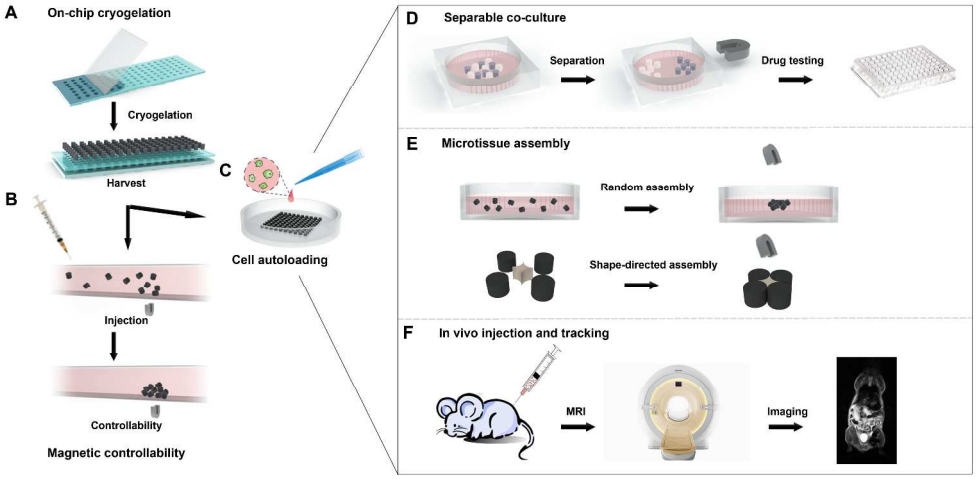

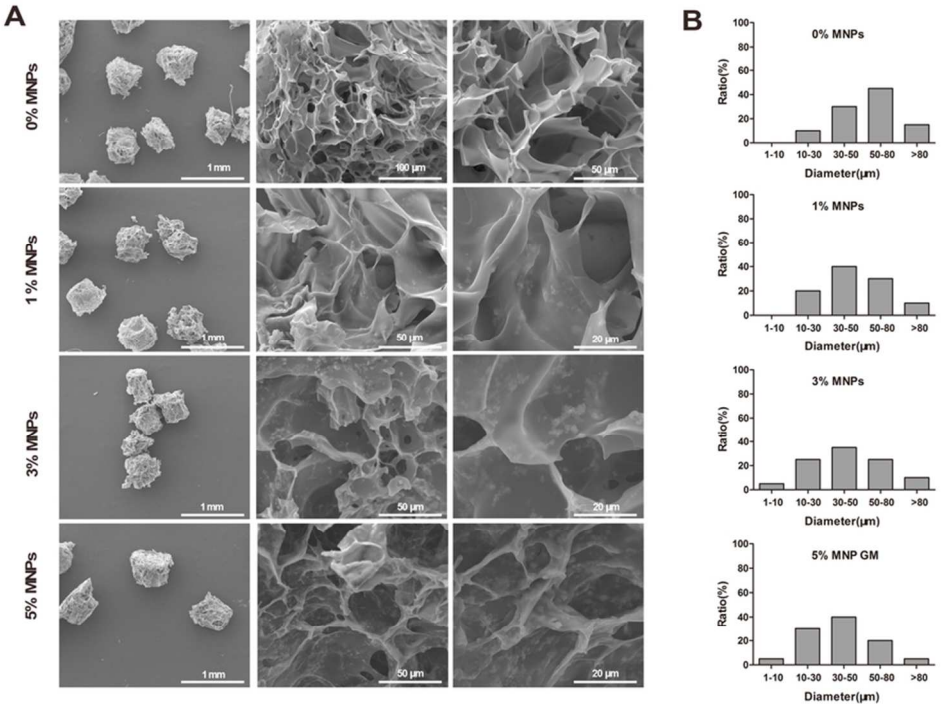

80x60mm (300 x 300 DPI)

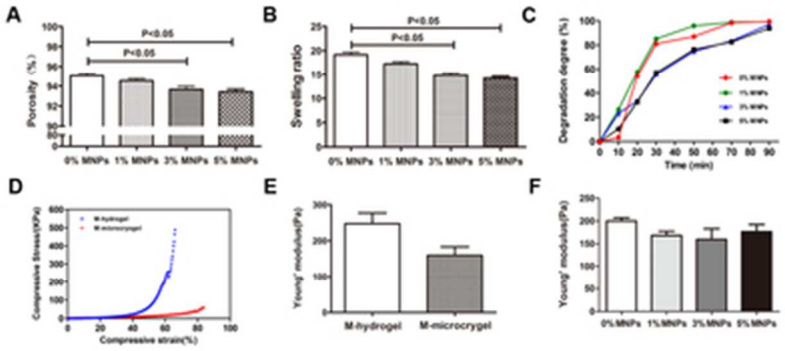

34x17mm (300 x 300 DPI)

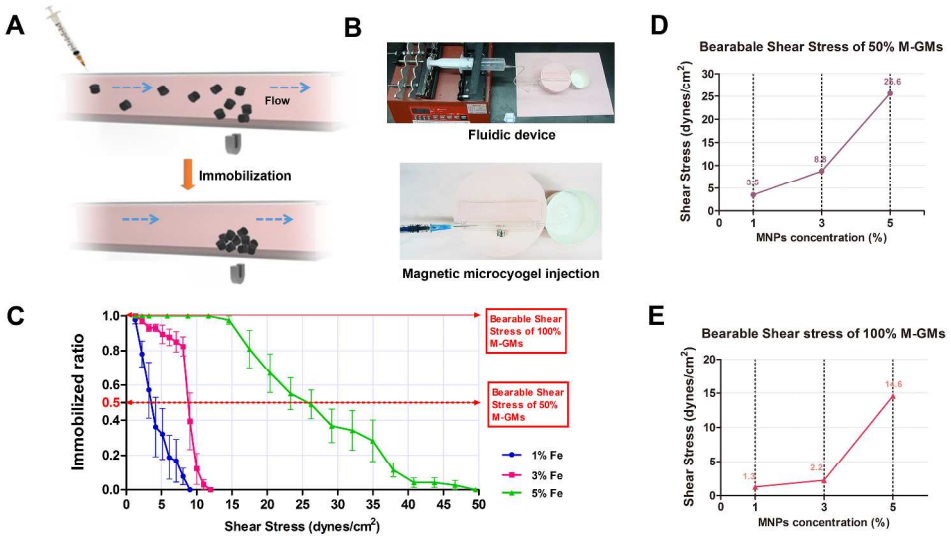

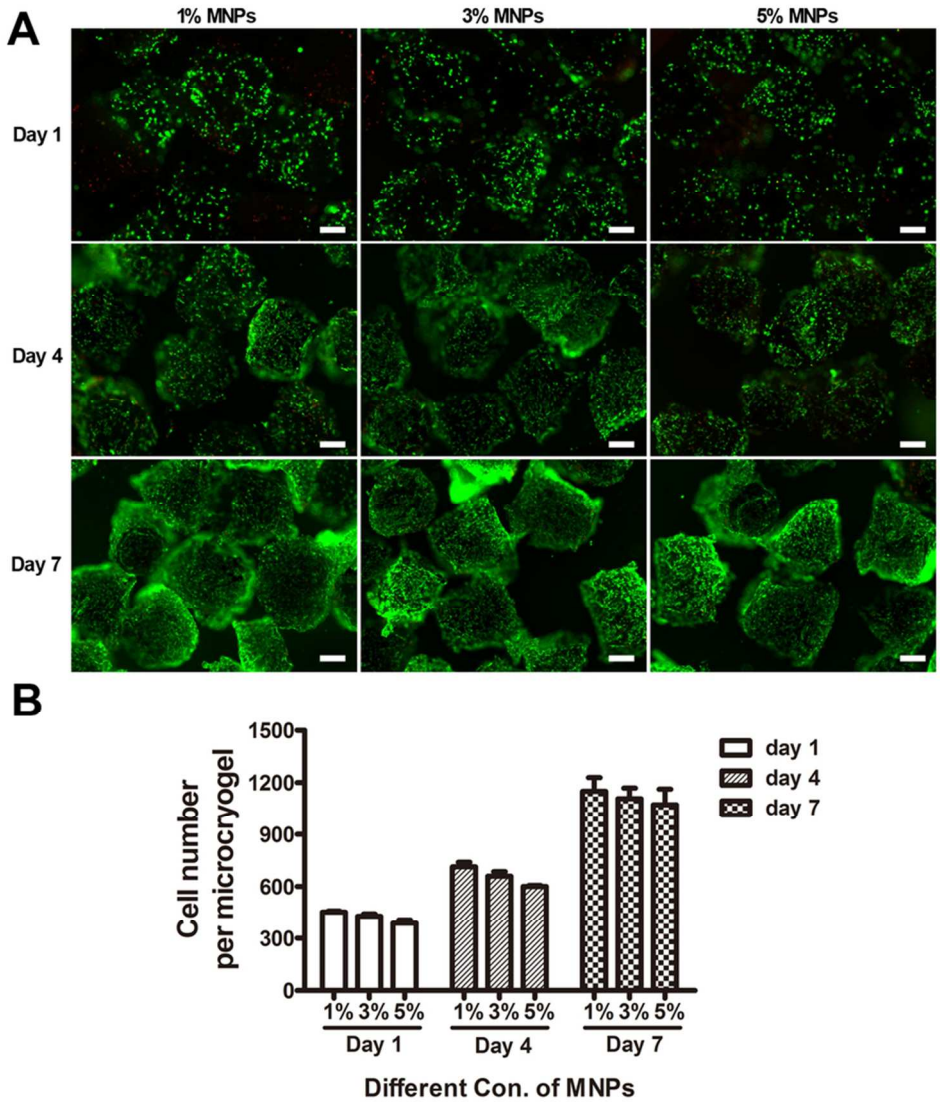

80x91mm (300 x 300 DPI)

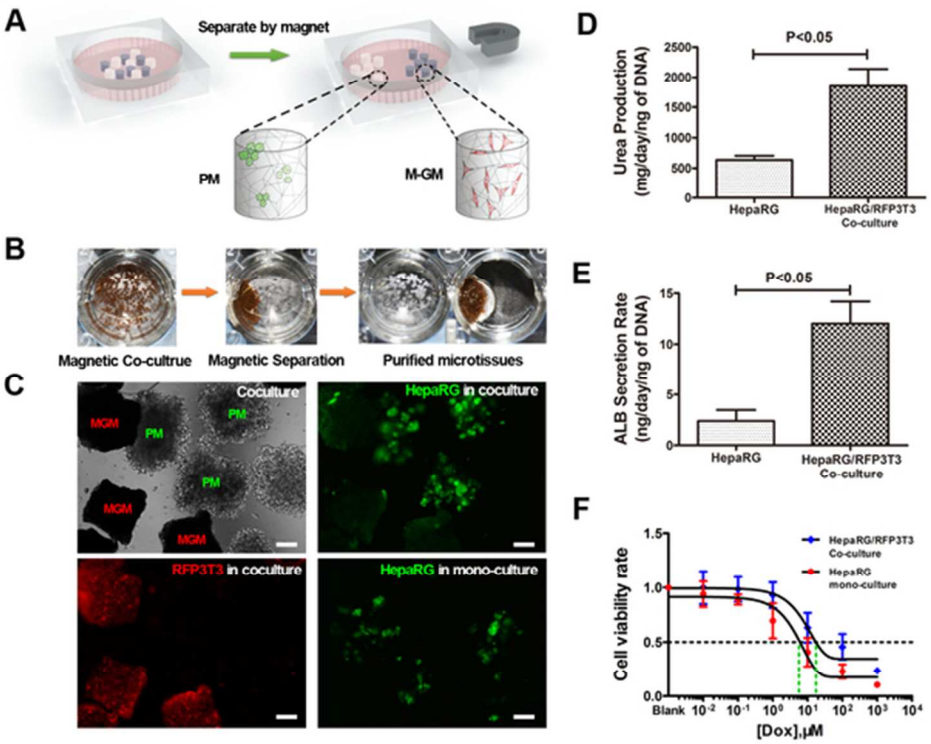

54x43mm (300 x 300 DPI)

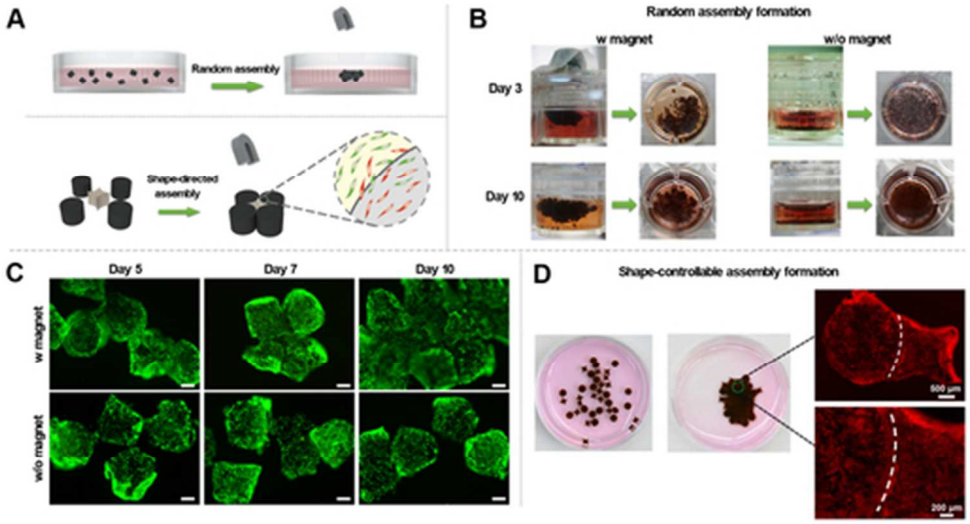

44x25mm (300 x 300 DPI)